Ligand-functionalized nanoparticles target endothelial cells in retinal capillaries after systemic application

Klaus Pollinger[a], Robert Hennig[a], Andreas Ohlmann[b], Rudolf Fuchshofer[b], Rebecca Wenzel[a], Miriam Breunig[a], Joerg Tessmar[a], Ernst R. Tamm[b], and Achim Goepferich[a,1]

[a]Department of Pharmaceutical Technology, and [b]Institute for Human Anatomy and Embryology, University of Regensburg, 93040 Regensburg, Germany

Edited by Robert Langer, Massachusetts Institute of Technology, Cambridge, MA, and approved March 4, 2013 (received for review November 21, 2012)

To date, diseases affecting vascular structures in the posterior eye are mostly treated by laser photocoagulation and multiple intraocular injections, procedures that destroy healthy tissue and can cause vision-threatening complications. To overcome these drawbacks, we investigate the feasibility of receptor-mediated nanoparticle targeting to capillary endothelial cells in the retina after i.v. application. Cell-binding studies using microvascular endothelial cells showed receptor-specific binding and cellular uptake of cyclo(RGDfC)-modified quantum dots via the αvβ3 integrin receptor. Conversely, Mueller cells and astrocytes, representing off-target cells located in the retina, revealed only negligible interaction with nanoparticles. In vivo experiments, using nude mice as the model organism, demonstrated a strong binding of the ligand-modified quantum dots in the choriocapillaris and intraretinal capillaries upon i.v. injection and 1-h circulation time. Nontargeted nanoparticles, in contrast, did not accumulate to a significant amount in the target tissue. The presented strategy of targeting integrin receptors in the retina could be of utmost value for future intervention in pathologies of the posterior eye, which are to date only accessible with difficulty.

age-related macular degeneration | diabetic retinopathy | choroid | neovascularization | ligand receptor interaction

Age-related macular degeneration (AMD) and diabetic retinopathy (DR) are among the leading causes of blindness (1, 2). AMD currently affects ~25 million (3) and DR 20–30 million people worldwide (4, 5). These figures will increase tremendously in the future due to the aging population (3) and the significant increase of diabetes patients (6), the majority of which are estimated to develop DR (7). Both AMD and DR cause a massive deterioration of blood vessels in the posterior segment of the eye, which ultimately causes blindness due to massive damage of the retina. The current standard therapies to treat such capillary-associated pathologies are laser photocoagulation and repeated intravitreal injections of antibodies against vascular endothelial growth factor (8–10). Both suffer from serious shortcomings: laser treatment inevitably destroys retinal tissue (11), and intraocular injections bear risks of endophthalmitis and retinal detachment, which both can lead to severe vision loss (12, 13).

We hypothesize that a nonintraocular pharmacotherapeutic intervention making use of receptor-mediated nanoparticle delivery to retinal capillary endothelial cells could be a highly promising alternative therapeutic option. Although preliminary results suggest that nanoparticles can be delivered to the αvβ3 integrin receptor following laser-induced choroidal neovascularization (14, 15), this disease model is not representative because it is typical of end-stage retinal pathologies. Here, capillaries are highly dislocated, leaky, subject to major remodeling processes, and accompanied by a massive αvβ3 integrin overexpression (16–18). Specific nanoparticle delivery, however, would be of utmost value in early stages of retinal diseases, such as diabetes-associated degenerative diseases (19) or inflammatory processes like uveitis (20), in which capillaries are still close to their native state and αvβ3 integrin expression is not substantially up-regulated (21, 22). Unfortunately, there is currently no evidence that i.v. injected nanoparticles can be addressed to such endothelial cells in the retina. Therefore, we address in the present study the question whether receptor-mediated nanoparticle delivery to endothelial cells of the retina is even possible in the "normal" eye because this specific nanoparticle cell interaction would open the door to preventive interventions in the future.

To this end, quantum dots (Qdots) with a fluorescence emission maximum at 655 nm were used as model nanoparticles because their optical properties make them ideal tools for analysis in biological media (23, 24). Cyclo(-Arg-Gly-Asp-D-Phe-Cys) [cyclo(RGDfC)] was immobilized on the particles as αvβ3 integrin-specific binding ligand (25). Following the fate of particles upon i.v. injection in mice, we explored whether nanoparticles can be delivered to retinal capillaries via this route.

Results and Discussion

In Vitro Binding Behavior of Nanoparticles. In the first step, cell selectivity and binding behavior of ligand-modified nanoparticles to important cell types residing in the posterior segment of the eye was investigated in vitro. Mueller cells and astrocytes, representing glial cells located in the retina (26, 27), and human dermal microvascular endothelial cells (HDMECs) as a model for retinal capillary endothelia were tested (Fig. 1). Being primary cells, we expected the chosen model cells to be reliable predictors for the in vivo binding of nanoparticles. For Mueller cells, only minute binding increase of cyclo(RGDfC)-Qdots compared with nontargeted Qdots was detectable in FACS measurements (Fig. 1*A*). Astrocytes did not show statistically significant binding of ligand-modified nanoparticles (Fig. 1*B*). For both cell types, nonspecific binding of unmodified nanoparticles was at a negligible level. For HDMECs, in contrast, a strong increase in Qdot binding after incubation with cyclo(RGDfC)-coupled nanoparticles was measured (Fig. 1*C*). This finding strongly suggests that a selective binding to these cells is indeed possible. Moreover, in light of the absence of cyclo(RGDfC)-Qdot binding to astrocytes and Mueller cells, a high binding selectivity to endothelial cells seems to be feasible. To verify that the nanoparticle–endothelial cell interaction was αvβ3 integrin mediated, a competitive displacement experiment using a 1,000-fold excess of free cyclo(RGDfC) was carried out. As a result, nanoparticle binding to HDMECs was suppressed to the level of nontargeted Qdots, giving clear evidence that it was indeed αvβ3 integrin mediated. In summary, the in vitro characterization suggests that cyclo(RGDfC)-modified nanoparticles are promising candidates for targeting endothelial cells in the posterior segment of the eye.

Author contributions: K.P., A.O., E.R.T., and A.G. designed research; K.P., R.H., A.O., and J.T. performed research; R.F. contributed new reagents/analytic tools; K.P., R.H., A.O., R.W., M.B., J.T., E.R.T., and A.G. analyzed data; and K.P. and A.G. wrote the paper.

The authors declare no conflict of interest.

This article is a PNAS Direct Submission.

[1]To whom correspondence should be addressed. E-mail: Achim.Goepferich@chemie.uni-regensburg.de.

This article contains supporting information online at www.pnas.org/lookup/suppl/doi:10.1073/pnas.1220281110/-/DCSupplemental.

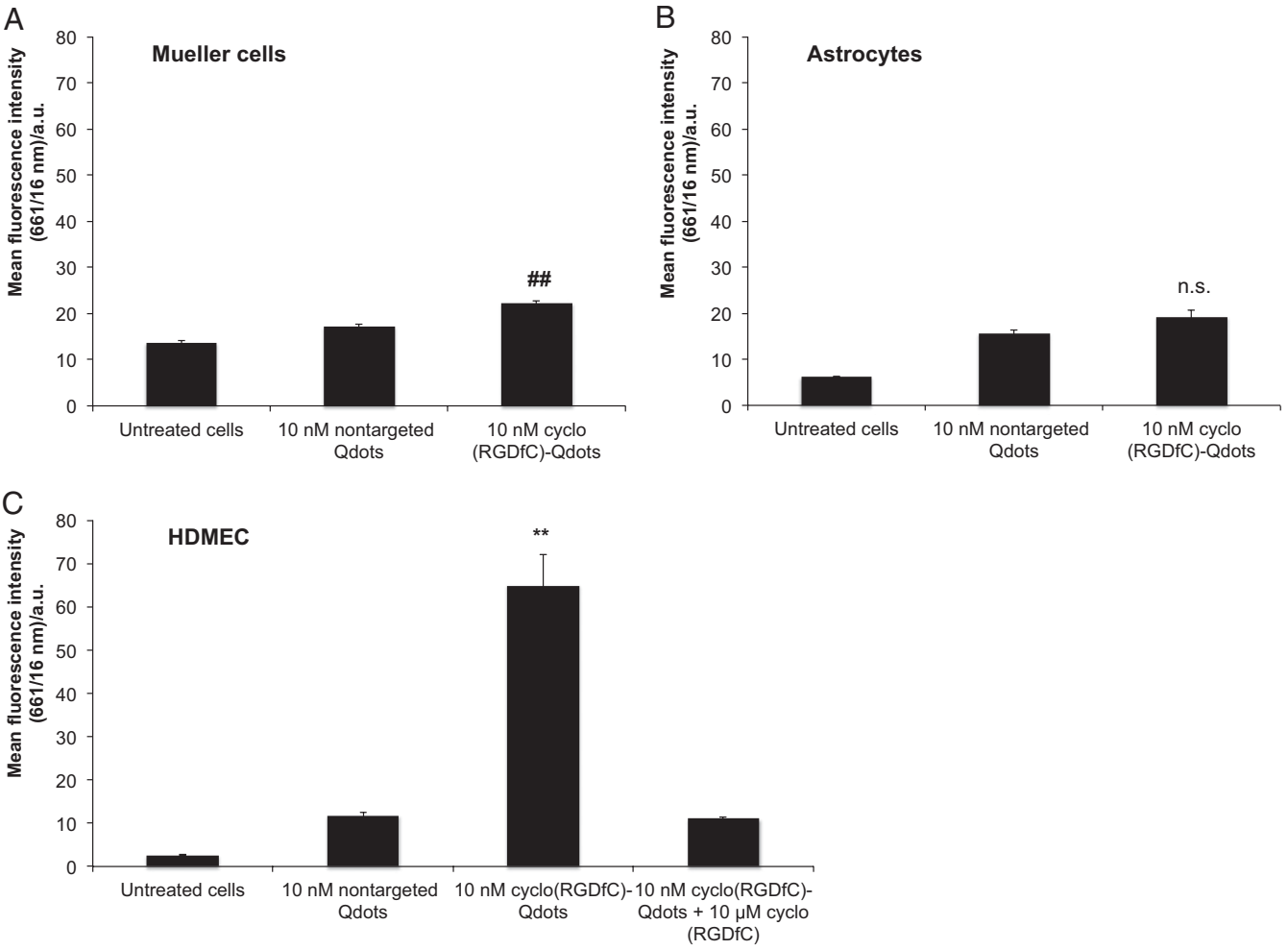

Fig. 1. Nanoparticle binding to important cells of the retina. Cell fluorescence measured by flow cytometry demonstrates only very weak binding of cyclo (RGDfC)-Qdots to Mueller cells and astrocytes (*A* and *B*). In contrast, HDMECs exhibit a strong interaction with cyclo(RGDfC)-Qdots (*C*). Coincubation with an excess of free cyclo(RGDfC) confirms the receptor-mediated nature of nanoparticle binding. The nonspecific binding of unmodified Qdots is low for all cell types. Levels of statistical significance are indicated as follows: $^{\#\#}P < 0.01$ comparing cyclo(RGDfC)-Qdots and nontargeted Qdots; $^{**}P < 0.01$ comparing cyclo (RGDfC)-Qdots with nontargeted Qdots and displacement. n.s., not significant comparing cyclo(RGDfC)-Qdots and nontargeted Qdots.

In Vitro Localization of Nanoparticles in the Cellular Context. To gain detailed insight into the interaction of nanoparticles with HDMECs, the binding properties were further studied by confocal microscopy (Fig. 2). Overall, the receptor-specific nanoparticle binding could be confirmed (Fig. 2*A*). Cyclo(RGDfC)-Qdots showed strong cell binding, whereas nonmodified Qdots yielded only low cell-associated fluorescence. Incubation with free cyclo(RGDfC) led to a displacement of ligand-coupled nanoparticles, giving evidence for αvβ3 integrin specific binding. To study the localization of cyclo(RGDfC)-Qdots inside the cells, z-stacks were taken (Fig. 2*B*). The distribution of fluorescence indicated that Qdots were located in vesicle-like structures. They were found throughout the cells, indicating an endocytotic uptake of nanoparticles into HDMECs as observed previously for other cell types (28–30).

To further investigate this localization of cyclo(RGDfC)-Qdots within the cells, counterstaining experiments with Alexa Fluor 488-labeled transferrin were carried out (Fig. 2*C*). Because transferrin is a standard marker for clathrin-mediated endocytosis, Alexa Fluor 488 transferrin fluorescence was located throughout the cells in endocytotic vesicles except for nuclei, which appeared as black spots in the center of the cells. Ligand-coupled nanoparticles showed a similar distribution pattern. Although a direct colocalization for nanoparticles and transferrin could not be observed, this finding clearly confirmed the cellular uptake of cyclo (RGDfC)-Qdots into HDMECs. The absence of colocalization can be most likely attributed to the fact that the αvβ3 integrin is, in contrast to transferrin, subjected to various endocytotic routes (31) and nanoparticles are additionally known to be able to alter endocytotic routes of the coupled ligands (29). The found internalization behavior of cyclo(RGDfC)-Qdots into HDMECs is highly promising because it could support the efficacy of drugs such as nucleic acids that are administered using nanoparticles and which can create therapeutic effects only inside the cell.

In summary, in vitro investigations gave clear evidence that receptor-mediated binding to αvβ3 integrins allows for selective nanoparticle binding to endothelial cells but not to retinal glial cells.

In Vivo Nanoparticle Detection in the Posterior Segment of the Eye. In the next step, nanoparticle distribution in the posterior segment of the eye after i.v. injection into the tail vein of nude mice was investigated. Here, the focus was on the presence of Qdots in the choriocapillaris and in intraretinal capillaries, as in vitro results clearly suggested binding of cyclo(RGDfC)-modified nanoparticles to endothelial cells. Initially, the detectability of Qdots in the highly pigmented surrounding tissue of the retina had to be evaluated. Confocal laser scanning microscopy in combination with spectral

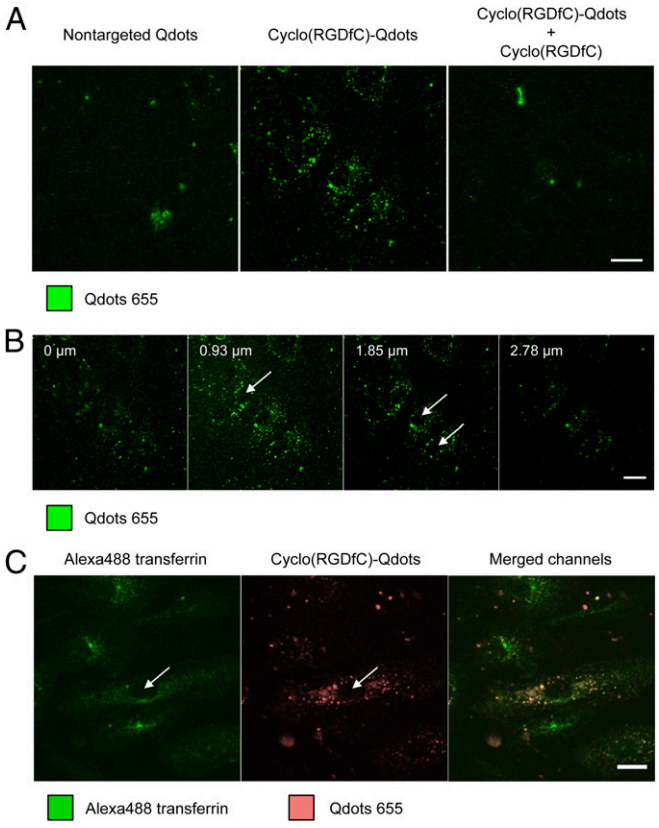

Fig. 2. Confocal microscopy analysis of Qdot distribution after binding to HDMECs. Qdots clearly show cyclo(RGDfC)-mediated binding to HDMECs in an αvβ3 integrin-dependent manner (*A*). Z-stack analysis shows a distribution of cyclo(RGDfC)-Qdots throughout the cells in dot-like structures leaving only nuclei unstained, which suggests internalization of nanoparticles (*B*). Counterstaining with Alexa Fluor 488-labeled transferrin confirmed the intracellular location of cyclo(RGDfC)-Qdots in HDMECs (*C*). Arrows mark selected nuclei. (Scale bar: 20 µm.)

analysis of the image section was used, as it facilitates the differentiation of tissue autofluorescence and Qdot fluorescence (Fig. 3). In the retina and the adjacent tissue of mice injected with nonmodified Qdots (Fig. 3*A*), autofluorescence of the surrounding tissue was detectable with a maximum intensity below 630 nm. In these mice, very few spots that show spectral properties of Qdots with a pronounced fluorescence emission maximum at 650 nm were found (Fig. 3*A*). This result indicated that pure PEG-coated nanoparticles show very little deposition in the posterior segment of the eye. For cyclo(RGDfC)-Qdots, a completely different picture was obtained (Fig. 3*B*). Here, Qdot fluorescence was detectable in high amounts. Fluorescence spectra ideally matching the fluorescence emission of Qdots 655 (Fig. 3*B*) were detected in strongly elevated amounts.

To assess the significance of our results with respect to the overall distribution of cyclo(RGDfC)-Qdots, their accumulation in different organs was briefly quantitatively analyzed (for details, see *Supporting Information*). As could be expected on the basis of previous studies with nonmodified (32, 33) as well as RGD-modified Qdots (34), the major part of the injected dose (ID) was sequestered into the liver and spleen (Table S1). Highly interesting was the particle content in the eye. When we calculated the particle content in the choroid, of which the choriocapillaris is only a part, we found 3.3% ID/g_{tissue}. This is higher than the content in the kidney (1.6% ID/g_{tissue}) and heart (1.5% ID/g_{tissue}) but comparable with the amount found in the lung (4.4% ID/g_{tissue}). These findings clearly reveal that a substantial amount of cyclo(RGDfC)-Qdots accumulates in the target tissue. A crucial factor influencing the distribution of nanoparticles is a sufficient blood half-life. Values of 30 min that were found for the nonmodified Qdots (33) are very well in line with 13% ID/g_{tissue} cyclo(RGDfC)-Qdots in the blood after 1 h of circulation (Table S1). Taken together, our results clearly indicate that the cyclo(RGDfC) modification of Qdots leads to a pronounced accumulation in the posterior eye.

In Vivo Localization of Nanoparticles Within the Posterior Eye Segment. Once we verified the presence of Qdots in the target tissue, we investigated the localization of nanoparticles by fluorescence microscopy. To gain a complete overview of the alignment of the different tissue layers in the posterior eye, nuclei were counterstained (Fig. 4). This procedure facilitated the localization of choroid, choriocapillaris, and retinal pigment epithelium (RPE), as well as retinal microvascular endothelial cells. This overview perfectly enabled localization of cyclo(RGDfC)-Qdots. Figure 4*A* confirms that ligand-modified nanoparticles accumulated considerably in the retina and adjacent tissue. Magnification of choriocapillaris and RPE shows major localization of nanoparticles at the endothelial cells of the choriocapillaris. Additionally, the micrographs suggest that small amounts could reside at the RPE. Furthermore, Qdots were found within intraretinal capillaries (Fig. 4*B*). These findings clearly suggest that nanoparticle modification with αvβ3 integrin-specific ligands indeed leads to a significant binding to endothelial cells in the posterior segment of the eye as suggested in vitro. The experiments further show that i.v.-administered nanoparticles could be a powerful tool for drug delivery to normal retinal vascular endothelial cells, which are not subject to serious remodeling processes.

This selective deposition in choriocapillaris and intraretinal capillaries could be of paramount value for future therapeutic applications in degenerative and inflammatory diseases of the posterior eye. Taking into consideration that expression of the αvβ3 integrin is elevated during neovascularization (35), the nanoparticle binding efficacy could be increased in pathologic situations of the retina. Even though the clinical potential of the presented nanoparticle blueprint still needs to be further explored, the effective targeting of the retina is an encouraging result for future nanomedical applications.

Conclusions

cyclo(RGDfC)-decorated nanoparticles can be targeted to endothelial cells in the posterior eye under physiological conditions. In contrast to the nonmodified control, targeted nanoparticles accumulated in the choriocapillaris and intraretinal capillaries. This distribution opens the door for future nanomedical applications to early stages of retinal diseases in which capillaries are subject to inflammatory processes and degeneration. In vitro experiments revealed strong αvβ3 integrin-mediated interaction of ligand-modified nanoparticles with HDMECs and substantial intracellular accumulation. These highly favorable characteristics could be of tremendous value for future therapeutic interventions and give a promising future perspective for a broad applicability of nanomedical targeting in the posterior segment of the eye.

Materials and Methods

Materials. Qdots 655 ITK amino PEG were obtained from Molecular Probes. Cyclo(RGDfC) was purchased from Bachem. Other chemicals were obtained from Sigma Aldrich at analytical grade or higher if not stated differently. HDMECs were purchased from PromoCell. Buffers used for peptide modification of Qdots were borate buffer pH 8.5 (10 mM $Na_2B_4O_7$) and PBS pH 7.4 (1.5 mM KH_2PO_4, 8 mM Na_2HPO_4, 2.7 mM KCl, 138 mM NaCl). Cell binding buffer pH 7.4 for in vitro studies was composed of 20 mM Tris, 150 mM NaCl, 2 mM $CaCl_2$, 1 mM $MnCl_2$, 1 mM $MgCl_2$, and 0.1% BSA (36). Four percent paraformaldehyde (PFA) solution pH 7.4 was prepared freshly in PBS, by dissolving PFA in preheated PBS (80 °C) and subsequent cooling on ice. Ultrapure water was obtained from a Milli-Q water purification system (Millipore).

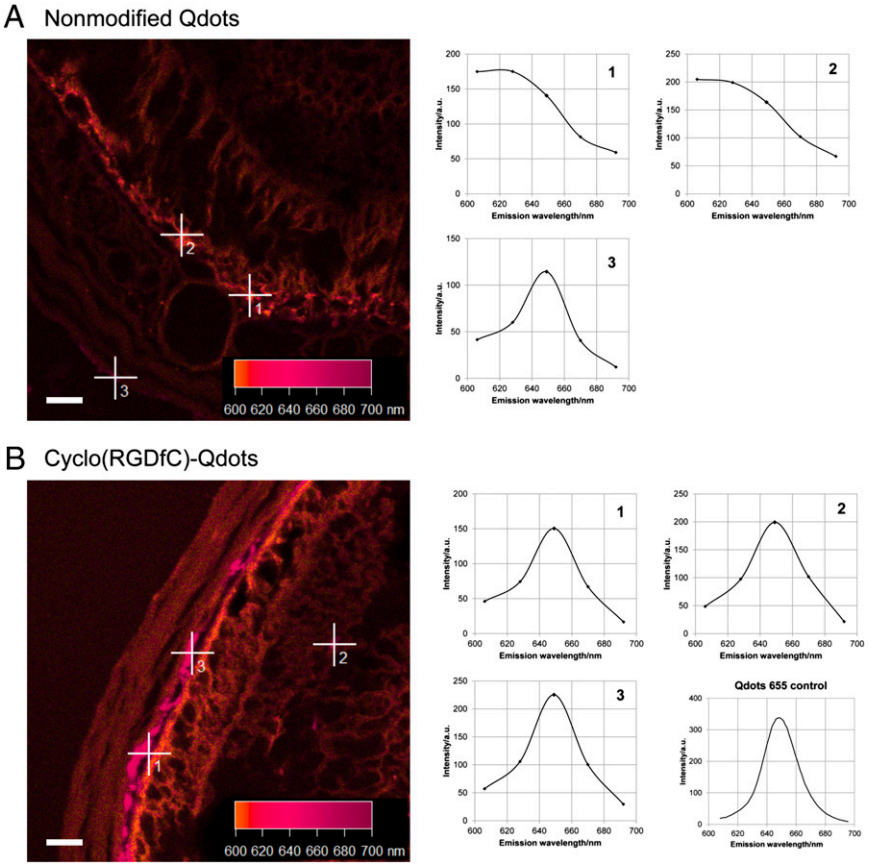

Fig. 3. Spectral analysis of representative micrographs showing retina and adjacent tissue. Tissue autofluorescence was determined to be below 620 nm (*A, 1* and *2*). After injection of nonmodified Qdots (*A*), only very few spots showing Qdot fluorescence (*A, 3*) were found. For cyclo(RGDfC)-Qdots (*B*), large amounts of spots, fitting the fluorescence properties of Qdots 655, were detected. (Scale bar: 20 μm.)

Nanoparticle Modification. For the manufacturing of cyclo(RGDfC)-coupled nanoparticles, Qdots with a fluorescence emission of 655 nm (Qdot 655 ITK amino PEG) were used as starting material. These Qdots consist of a CdSe core with a ZnS shell and carry a polymer coating, which mediates water dispersability. On top of this polymeric coating, amine-terminated polyethyleneglycol (PEG) is coupled, allowing for covalent surface modification of the nanocrystals. In doing so, sulfosuccinimidyl-4-(*N*-maleimidomethyl)cyclohexane-1-carboxylate (sulfo-SMCC) (Thermo Fisher) was used as a heterobifunctional linker to couple the thiol group of cyclo(RGDfC) to the nanoparticle surface. In the first reaction step, Qdots were allowed to react with a 1,000-fold molar excess of sulfo-SMCC in borate buffer pH 8.5 for 1 h to induce thiol reactivity. Subsequently, excess linker was removed by gel filtration chromatography (GFC) using a Sephadex G-25 resin in a PD-10 column (1.45 × 5.0 cm) (GE-Healthcare) and PBS pH 7.4 as elution buffer. In the next step, cyclo(RGDfC) was added to the purified, maleimide-activated Qdots in a 100-fold molar excess and reacted for 1 h to form a thioether bond with the maleimides on the nanoparticle surface. Before addition to the activated Qdots, cyclo (RGDfC) was reduced to cleave disulfide bonds using Tris(2-carboxyethyl) phosphine, at a concentration of 5 mM. After the reaction of Qdots with cyclo (RGDfC), nonreacted maleimide groups on the nanoparticle surface were inactivated by reaction with a 100-fold molar excess of 2-mercaptoethanol for 30 min. Afterward, the reaction mixture was purified of the excess peptide and 2-mercaptoethanol by GFC as described above. Finally, the Qdots were concentrated by ultrafiltration using a 100-kDa cutoff Amicon Ultra-4 filter unit (Milipore) for 10 min at 2,000 × *g*. Qdot concentration was measured by fluorimetric measurement in 96-well plates on an LS-55 fluorescence spectrometer (Perkin-Elmer) using an excitation wavelength of 450 nm and an emission wavelength of 655 nm (37).

Nanoparticles that are referred to as "nontargeted Qdots" were prepared as described above without addition of cyclo(RGDfC).

Fluorescence Measurements. Fluorescence spectra were taken using an LS-55 fluorescence spectrometer (Perkin-Elmer). For reference spectra of Qdots 655, an excitation wavelength of 450 nm was applied, and fluorescence emission was acquired from 600 to 700 nm.

Cell Culture. HDMECs were cultured in supplemented endothelial cell growth medium MV (Promocell). Mueller cells were grown in DMEM with high glucose (4.5 g/L) and stable glutamine (PAA), supplemented with 100 U penicillin/mL, 100 μg streptomycin/mL, and 10% (vol/vol) FBS (Life Technologies). Astrocytes were cultured in DMEM with 100 U penicillin/mL, 100 μg streptomycin/mL, and 10% (vol/vol) FBS. All cells were kept in T75 culture flasks (Corning) and maintained in incubators at 37 °C with 5% (vol/vol) CO_2 and 95% relative humidity.

Isolation of Mueller Cells. Isolation and initiation of primary cultures from purified Mueller cells were performed as previously described (38). In brief, eyes of 8- to 10-d-old Wistar rats were enucleated and placed in DMEM containing 10% (vol/vol) FBS, gentamycin (20 μg/mL), penicillin (100 U/mL), and streptomycin (100 μg/mL) overnight. The next day, the eyes were incubated for 30 min at 37 °C in DMEM containing 0.1% trypsin (PAA) and 70 U/mL collagenase, followed by an additional incubation in DMEM with 10% (vol/vol) FBS. Subsequently, the retina was dissected from the rest of the ocular tissue and chopped into 1-mm^2 fragments. Six to eight retinal fragments were transferred into a 35-mm cell culture dish, covered with a sterile glass coverslip, and incubated in DMEM containing 10% (vol/vol) FBS, gentamycin (20 μg/mL), penicillin (100 U/mL), and streptomycin (100 μg/mL) at 37 °C in humidified 5% (vol/vol) CO_2. When cell outgrowth reached local semiconfluency, retinal aggregates and debris were removed by forcibly pipetting medium onto the dish. This procedure was repeated until all aggregates were removed, as judged by examination under an inverse phase contrast microscope (Zeiss). After isolated Mueller cells reached confluency, the cells were passaged two times before the experiments were performed.

Isolation of Astrocytes. Isolation and initiation of primary cultures of human optic nerve head (ONH) astrocytes were performed as previously described

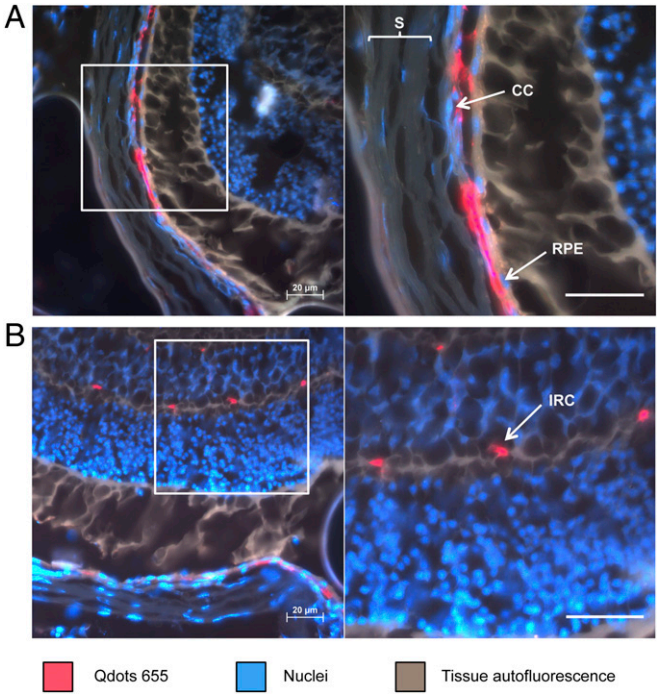

Fig. 4. Investigation of cyclo(RGDfC)-Qdot location in the posterior segment of the eye. The major part of Qdots is clearly located associated to the endothelia in the choriocapillaris (*A*). Further accumulation of cyclo(RGDfC)-Qdots was detectable in intraretinal capillaries (*B*). CC, choriocapillaris; IRC, intraretinal capillaries; RPE, retinal pigment epithelium; S, sclera. (Scale bars: 20 μm.)

(39). In brief, eyes were cut equatorially behind the ora serrata, and the ONH was isolated from the neighboring tissues. Discs of lamina cribrosa were prepared by dissection from the pre- and postlaminar regions and were subsequently chopped and placed in Petri dishes with 2 mL DMEM/F-12 supplemented with 10% (vol/vol) FBS, 5 ng/mL human basic pituitary fibroblast growth factor (bFGF), 5 ng/mL human platelet-derived growth factor-A chain (PDGFAA), and 50 U/mL penicillin and 50 μg/mL streptomycin (Life Technologies). The medium was changed every second day, and cells were passaged in a ratio of 1:2, using 0.1% trypsin and 0.02% EDTA in phosphate-buffered 0.15 M NaCl (pH 7.2) (Life Technologies). Astrocytes were characterized by immunohistochemical staining with antibodies against glial fibrillary acidic protein (GFAP, 1:100, rabbit anti-human GFAP). Only GFAP-positive cultures were used for further experiments. Methods of securing human tissue were humane, included proper consent and approval, and complied with the Declaration of Helsinki.

Flow Cytometry (FACS). Flow cytometric nanoparticle binding assays were carried out using a FACSCalibur flow cytometer (Becton Dickinson). Cells were seeded into 24-well plates (Corning) by using the cell culture media described above. Astrocytes (passage 10) and HDMECs (passage 13) were plated at a density of 120,000 cells per well, whereas Mueller cells (passage 3) were plated at 95,000 cells per well. After cultivation for 24 h, cells were incubated with cyclo(RGDfC)-coupled Qdots or nontargeted nanoparticles at a concentration of 10 nM in cell binding buffer for 1 h at 37 °C. To investigate the $\alpha v\beta 3$ integrin-mediated interaction of cyclo(RGDfC)-Qdots with the cells, nanoparticle incubation was carried out in the presence of a 1,000-fold molar excess of free cyclo(RGDfC) as a competitor. After incubation, cell binding buffer containing test substances was removed, and cells were washed with PBS (37 °C). Subsequently, cells were detached from the cell culture dish using a 0.25% trypsin solution (37 °C) and centrifuged (5 min, 200 × *g*). Then, cells were washed again with ice-cooled PBS, centrifuged (5 min, 200 × *g*), and resuspended in ice-cooled PBS. Afterward, cell-associated fluorescence was analyzed by flow cytometry. Here, Qdot fluorescence was excited at 488 nm, and emission was acquired using a 661/16 nm bandpass filter.

FACS data were acquired with the BD CellQuest pro software (Becton Dickinson) and analyzed using WinMDI 2.9 (The Scripps Research Institute). The population of intact cells was gated, and the geometrical mean of fluorescence intensity was determined from the histogram.

Microscopic Analysis of Cultured Cells. For microscopic analysis of nanoparticle binding behavior, HDMECs were seeded in eight-well chamber slides (μ-slide eight-well, 1-cm^2 culture area; Ibidi) at a density of 5,000 cells per well, using the corresponding cell culture media. After culturing for 24 h, cells were incubated with a concentration of 10 nM of differently grafted Qdots in cell binding buffer for 30 min at 37 °C. For counterstaining of endocytotic vesicles, Alexa Fluor 488-conjugated transferrin (Life Technologies) was added to the incubation buffer at a concentration of 3 μg/mL. After incubation, solutions containing test substances were replaced by fresh cell binding buffer. Subsequently, cells were examined under a Zeiss Axiovert 200 microscope combined with a LSM 510 laser-scanning device using a 63× Plan-Apochromat (NA 1.4) objective (Zeiss). Qdot fluorescence and Alexa Fluor 488 were excited using an Ar-laser at 488 nm. Fluorescence emission of Qdots was acquired using a 650-nm longpass filter, and Alexa Fluor 488 emission was detected using a 505- to 530-nm bandpass filter. The pinhole was adjusted to obtain a focal plane of 1.1 μm. Qdot fluorescence was displayed either in false color green or light red to improve visibility. Alexa Fluor 488-conjugated transferrin was displayed in false color green.

The software used for image acquisition and processing was AIM 4.2 (Zeiss).

Animal Experiments. Male NMRI (nu/nu) mice aged from 3 to 4 mo and weighing around 30 g were used as model animals. Mice were bred in-house at the animal laboratories of the University of Regensburg under specified pathogen free conditions. Before the experiments, mice were anesthetized by i.p. injection of 50 μL of a mixture of ketamine and xylazine (three parts ketamine and one part xylazine by volume). After prewarming the tail in water (~45 °C), Qdots were injected into the lateral tail vein. The amount of injected Qdots was 200 pmol in a volume of 50–100 μL of PBS. After 1 h of circulation in the blood, mice were killed by cervical dislocation and the eyes were enucleated.

All animal experiments were carried out according to the national and institutional guidelines and were approved by the local authority (Regierung der Oberpfalz, reference no. 54–2532,1–23/11).

Microscopic Analysis of Tissue Sections. Immediately after removal, eyes were fixed in a solution of 4% (mass/vol) PFA for 4 h at room temperature. Subsequently, they were briefly washed with PBS, embedded in Tissue Tek O.C.T. Compound (Sakura Finetek) using Cryomold embedding molds (Sakura Finetek) and finally frozen in the gas phase of liquid nitrogen. Thereafter, specimens were cut into 10-μm-thick sections using an HM 500 OM microtome (Microm International), transferred onto glass slides (Superfrost plus; Thermo Scientific), and mounted with Vectashield mounting medium supplemented with DAPI (Vector Laboratories). The tissue sections were examined using a Zeiss Axiovert 200 inverted microscope (Zeiss) combined with an LSM 510 laser-scanning device. The objectives used were a 40× Plan-Neofluar (NA 1.3) and a 63× Plan-Apochromat (NA 1.4) (Zeiss).

For spectral analysis of Qdot fluorescence in tissue sections, the excitation wavelength was 488 nm, and the emitted light was detected using a Zeiss meta detector (Zeiss). The focal plane was adjusted to 3.1 μm. The acquired wavelength stacks were displayed as color-coded pictures, with different colors representing different wavelengths. The software used for image acquisition and processing was AIM 4.2 (Zeiss).

In nonconfocal fluorescence microscopy experiments, specimens were exposed to a mercury-vapor lamp (Zeiss). For simultaneous acquisition of Qdot and DAPI fluorescence, a filter with an excitation maximum of 365 nm, a beam splitter at 395 nm, and longpass emission above 420 nm was applied. The software used for image acquisition and processing was AxioVision 4.6 (Zeiss).

Statistics. One-way analysis of variances (ANOVA) was carried out combined with a multiple comparisons test (Tukey's test) to assess statistical significance. Levels of significance were set as indicated.

ACKNOWLEDGMENTS. We thank Dr. Thilo Spruss and Franz Wiesenmayer for their assistance in animal experiments, Margit Schimmel and Elke Stauber for support in tissue preparation, and Renate Liebl for assistance in cell culture. Furthermore, we thank Kelsey Knewtson for carefully revising this manuscript. This work was supported by Deutsche Forschungsgemeinschaft Grant GO565/17-1 and Teilprojekt 7 of Research Unit (Forschergruppe) 1075.

1. Coorey NJ, Shen W, Chung SH, Zhu L, Gillies MC (2012) The role of glia in retinal vascular disease. *Clin Exp Optom* 95(3):266–281.
2. Lee J-H, Pidaparti RM, Atkinson GM, Moorthy RS (2012) Design of an implantable device for ocular drug delivery. *J Drug Deliv* 2012:527516.
3. Chopdar A, Chakravarthy U, Verma D (2003) Age related macular degeneration. *BMJ* 326(7387):485–488.
4. Charbonnel B, Dormandy J, Erdmann E, Massi-Benedetti M, Skene A; PROactive Study Group (2004) The prospective pioglitazone clinical trial in macrovascular events (PROactive): Can pioglitazone reduce cardiovascular events in diabetes? Study design and baseline characteristics of 5238 patients. *Diabetes Care* 27(7):1647–1653.
5. Meleth AD, et al. (2005) Serum inflammatory markers in diabetic retinopathy. *Invest Ophthalmol Vis Sci* 46(11):4295–4301.
6. Wild S, Roglic G, Green A, Sicree R, King H (2004) Global prevalence of diabetes: Estimates for the year 2000 and projections for 2030. *Diabetes Care* 27(5):1047–1053.
7. Sivaprasad S, Gupta B, Crosby-Nwaobi R, Evans J (2012) Prevalence of diabetic retinopathy in various ethnic groups: A worldwide perspective. *Surv Ophthalmol* 57(4): 347–370.
8. Giuliari GP (2012) Diabetic retinopathy: Current and new treatment options. *Curr Diabetes Rev* 8(1):32–41.
9. Kumar B, Gupta SK, Saxena R, Srivastava S (2012) Current trends in the pharmacotherapy of diabetic retinopathy. *J Postgrad Med* 58(2):132–139.
10. Avery RL, et al. (2006) Intravitreal bevacizumab (Avastin) for neovascular age-related macular degeneration. *Ophthalmology* 113(3):363–372, e5.
11. Maeshima K, Utsugi-Sutoh N, Otani T, Kishi S (2004) Progressive enlargement of scattered photocoagulation scars in diabetic retinopathy. *Retina* 24(4):507–511.
12. Martidis A, et al. (2002) Intravitreal triamcinolone for refractory diabetic macular edema. *Ophthalmology* 109(5):920–927.
13. Moshfeghi DM, et al. (2003) Acute endophthalmitis following intravitreal triamcinolone acetonide injection. *Am J Ophthalmol* 136(5):791–796.
14. Singh SR, et al. (2009) Intravenous transferrin, RGD peptide and dual-targeted nanoparticles enhance anti-VEGF intraceptor gene delivery to laser-induced CNV. *Gene Ther* 16(5):645–659.
15. Salehi-Had H, et al. (2011) Utilizing targeted gene therapy with nanoparticles binding alpha v beta 3 for imaging and treating choroidal neovascularization. *PLoS ONE* 6(4): e18864.
16. Krzystolik MG, et al. (2002) Prevention of experimental choroidal neovascularization with intravitreal anti-vascular endothelial growth factor antibody fragment. *Arch Ophthalmol* 120(3):338–346.
17. Spilsbury K, Garrett KL, Shen WY, Constable IJ, Rakoczy PE (2000) Overexpression of vascular endothelial growth factor (VEGF) in the retinal pigment epithelium leads to the development of choroidal neovascularization. *Am J Pathol* 157(1):135–144.
18. Yoshida T, Gong J, Xu Z, Wei Y, Duh EJ (2012) Inhibition of pathological retinal angiogenesis by the integrin $\alpha v\beta 3$ antagonist tetraiodothyroacetic acid (tetrac). *Exp Eye Res* 94(1):41–48.
19. Vincent JA, Mohr S (2007) Inhibition of caspase-1/interleukin-1beta signaling prevents degeneration of retinal capillaries in diabetes and galactosemia. *Diabetes* 56(1): 224–230.
20. Gomes Bittencourt M, et al. (2012) New treatment options for noninfectious uveitis. *Dev Ophthalmol* 51:134–161.
21. Hodivala-Dilke K (2008) alphavbeta3 integrin and angiogenesis: A moody integrin in a changing environment. *Curr Opin Cell Biol* 20(5):514–519.
22. Eliceiri BP, Cheresh DA (1999) The role of alphav integrins during angiogenesis: Insights into potential mechanisms of action and clinical development. *J Clin Invest* 103(9):1227–1230.
23. Hild WA, Breunig M, Goepferich A (2008) Quantum dots: Nano-sized probes for the exploration of cellular and intracellular targeting. *Eur J Pharm Biopharm* 68(2): 153–168.
24. Walling MA, Novak JA, Shepard JRE (2009) Quantum dots for live cell and in vivo imaging. *Int J Mol Sci* 10(2):441–491.
25. Aumailley M, et al. (1991) Arg-Gly-Asp constrained within cyclic pentapeptides. Strong and selective inhibitors of cell adhesion to vitronectin and laminin fragment P1. *FEBS Lett* 291(1):50–54.
26. Franze K, et al. (2007) Muller cells are living optical fibers in the vertebrate retina. *Proc Natl Acad Sci USA* 104(20):8287–8292.
27. Newman EA (2003) New roles for astrocytes: Regulation of synaptic transmission. *Trends Neurosci* 26(10):536–542.
28. Zhang LW, Monteiro-Riviere NA (2009) Mechanisms of quantum dot nanoparticle cellular uptake. *Toxicol Sci* 110(1):138–155.
29. Tekle C, Deurs Bv, Sandvig K, Iversen T-G (2008) Cellular trafficking of quantum dot-ligand bioconjugates and their induction of changes in normal routing of unconjugated ligands. *Nano Lett* 8(7):1858–1865.
30. Ferreira L, et al. (2008) Human embryoid bodies containing nano- and microparticulate delivery vehicles. *Adv Mater (Deerfield Beach Fla)* 20:2285–2291.
31. Ivaska J, Heino J (2011) Cooperation between integrins and growth factor receptors in signaling and endocytosis. *Annu Rev Cell Dev Biol* 27:291–320.
32. Schipper ML, et al. (2007) microPET-based biodistribution of quantum dots in living mice. *J Nucl Med* 48(9):1511–1518.
33. Praetner M, et al. (2010) The contribution of the capillary endothelium to blood clearance and tissue deposition of anionic quantum dots in vivo. *Biomaterials* 31(26): 6692–6700.
34. Cai W, et al. (2006) Peptide-labeled near-infrared quantum dots for imaging tumor vasculature in living subjects. *Nano Lett* 6(4):669–676.
35. Haubner R, et al. (2005) Noninvasive visualization of the activated alphavbeta3 integrin in cancer patients by positron emission tomography and [18F]Galacto-RGD. *PLoS Med* 2(3):e70.
36. Shi W, Bartlett JS (2003) RGD inclusion in VP3 provides adeno-associated virus type 2 (AAV2)-based vectors with a heparan sulfate-independent cell entry mechanism. *Mol Ther* 7(4):515–525.
37. Cai W, Chen X (2008) Preparation of peptide-conjugated quantum dots for tumor vasculature-targeted imaging. *Nat Protoc* 3(1):89–96.
38. Seitz R, Hackl S, Seibuchner T, Tamm ER, Ohlmann A (2010) Norrin mediates neuroprotective effects on retinal ganglion cells via activation of the Wnt/beta-catenin signaling pathway and the induction of neuroprotective growth factors in Muller cells. *J Neurosci* 30(17):5998–6010.
39. Fuchshofer R, Birke M, Welge-Lussen U, Kook D, Lütjen-Drecoll E (2005) Transforming growth factor-beta 2 modulated extracellular matrix component expression in cultured human optic nerve head astrocytes. *Invest Ophthalmol Vis Sci* 46(2):568–578.